THE ISOCAM FLAT FIELD CALIBRATION REPORT

A. Biviano[1,2], J. Blommaert[1], O. Laurent[3], K. Okumura[1], R. Siebenmorgen[1]
B. Altieri[1], O. Boulade[3], P. Gallais[1,3], L. Metcalfe[1], S. Ott[1]

1: CAM IDT, ESA Satellite Tracking Station, PO Box 50727, E-28080 Madrid, Spain
2: Osservatorio Astronomico di Trieste, via G.B. Tiepolo 11, I-34131 Trieste, Italy
3: CEA, DSM/DAPNIA/SAp, CE-Saclay, F-91191, Gif-sur-Yvette Cedex, France

Version 1.1 – May 19^{th}, 1998

Abstract

We describe the calibration, measurements and data reduction, of the flat fields of ISOCAM. The observations were done either on the sky, on selected zodiacal background regions of maximum brightness, or internally with the Internal Calibration Device (ICD). The SW detector flat-fields, in particular, are entirely based on measurements done with the ICD, because at short wavelengths the zodiacal background is not bright enough.

We analyse the main factors limiting the final accuracy of the calibration flat-fields. We show that when the zodiacal background flux is high, the main source of noise in the flat-field observations come from the non-uniform transient behaviours of different pixels. On the other hand, in the case that the zodiacal background flat-fields are Poisson-noise dominated, we consider and discuss the merits of alternative strategies for flat-fielding, such as using the ICD, or adopting a given filter flat-field for other filters.

We conclude that the calibration observations have yielded flat-fields to an accuracy similar to pre-launch expectations.

1 Introduction

In this document we describe the calibration of the flat-fields of the CAM SW and LW detectors.

The flat-field (FF hereafter) can be defined as the relative response of different pixels of the detector to a source of uniform brightness distribution within the field-of-view (FOV hereafter).

It is useful to distinguish between the *detector flat* and the *optical flat* (hereafter DF and OF, respectively). The DF can be defined as the relative response of different pixels to a uniform illumination of the detector, while the OF can be defined as the relative flux falling onto different pixels when a source of uniform brightness distribution occupies the FOV. The *observed* FF results from the product of the DF by the OF.

In other words, while the DF is strictly related to the relative sensitivity of the detector pixels to incoming flux, the OF measures the vignetting due to the optical components of the camera, in particular the aperture stops near the filters. The vignetting profile is a function of the angular distance from the optical axis, and with different lens magnifications the detector sees different parts of the vignetting profile. On top of that, even with the same lens, a change in the OF occurs because of the lens wheel jitter (see § 4).

In practice, the DF is not directly observable. So, by convention, the FF at 1.5″ is defined to be the DF, for any given filter, because it suffers less than other PFOV FFs from vignetting effects. The OFs at any PFOV are obtained by dividing the observed FFs by the appropriate filter DF. As a consequence, the OF at 1.5″ is a matrix with 1's everywhere.

Flat-fielding is a crucial step in the data-processing, in particular in the IR bands, where the brightness of the background is very often comparable to (or higher than) the brightness of the target source. Therefore, the calibration of FFs is an essential step in the overall calibration strategy of ISO-CAM. It must be noted, however, that many observations in raster and beam-switch mode (see "ISOCAM Observer's Manual") allow the observer to directly build a FF from his data, depending on the brightness of the background, and the relative extension of the target source(s) and the raster (or beam-switching) step(s). In all staring mode observations, as well as in a few cases of raster and beam-switching observations, particularly of very extended sources or crowded fields, the use of a library FF is nevertheless unavoidable.

In the following, we will discuss the calibration observations and data reduction (§ 2), the evolution of FFs throughout the ISO mission (§ 3), the characteristics of the calibration FFs (§ 4). In § 5 we provide a detailed analysis of the error budget in the calibration of FFs, and in § 6 we discuss the best possible approaches to flat-fielding, based on the available calibration data. We give our summary and conclusions in § 7.

2 The data

2.1 Observations

There have been two kinds of FF observations:

1. observations on the zodiacal background, that we call "ZB observations" in the following;
2. observations with the Internal Calibration Device, which we will refer to as "ICD measurements".

The targets for ZB observations were chosen as close as possible to the sun-viewing constraint of ISO (see "ISO Observer's Manual"), in order to maximize their flux. In Fig. 1 we show an example of how the position of the target would have been chosen in the case of revolution ("rev." hereafter) 333. The sun constraint is indicated by asterisks in the figure, and the zodiacal zone by crosses. It can be seen that in this case it is not possible to choose a target in the vicinity of the sun constraint *and* in the zodiacal region, because of the earth constraint at low right ascensions (indicated by triangles), and of the galactic center position at high right ascension (indicated by diamonds). The best choice would then be to choose the FF target near the anti-sun constraint (again indicated by asterisks, but at the two edges of the figure, instead than at the center), at high right ascension (since at low right ascensions this is again not possible because of the earth constraint).

The ZB observations have been done in raster mode, at integration times (T_{int}, hereafter) of 2 seconds ("s" hereafter) during the PV-phase, and 5 and 10 s during the Routine-phase, and at all PFOVs, for a total of $\simeq$ 1600 s per raster observation, except for two very long rasters in the filters LW10 and LW3, done in rev.s 22 and 286, respectively, and lasting $\simeq$ 8000 s.

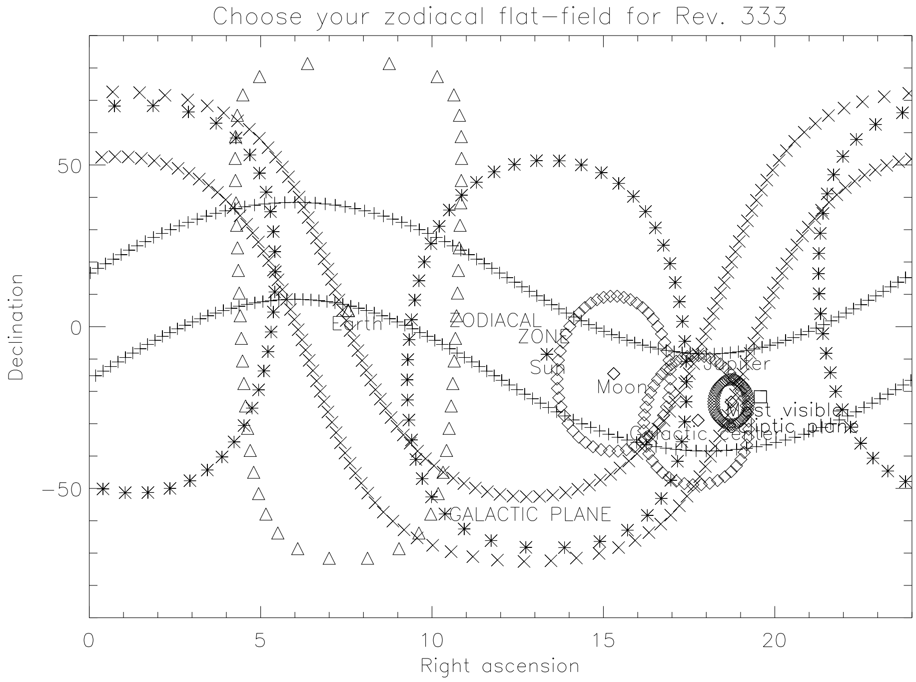

Figure 1: An example of the zodiacal light target visibility for revolution 333. For more details, see the text.

The choice of the raster strategy of observation allows to minimize eventual non-uniformities in the zodiacal background, since a given pixel of the detector sees different sky pixels during the raster, and a FF image can be constructed by the median of all raster-position images.

A total of $\sim$ 100 zodiacal background raster observations have been executed in the available CAM calibration time, allowing an extensive data-base of FFs to be built, as well as a monitoring of eventual FF drifts during the mission.

In Fig. 2 we show four examples of ZB FFs in the LW3 filter, at 1.5$''$, and 3$''$, 6$''$ and 12$''$, in normalised units (see below). It can be seen that only the central part of the array is illuminated when the 12$''$PFOV is chosen. Note also the characteristic filamentary feature that crosses the array from left to right at the top of the image (usually nicknamed: "the hair").

All of these ZB observations, except one, were done using the LW channel of CAM. Indeed, even with an accurate choice of the highest brightness zodiacal targets, in some CAM configurations these targets do not provide enough incident flux for a proper calibration. This is the case, in particular, for the short-wavelength, small-PFOV configurations of LW, and for all the SW configurations. The only solution in this case is to use the ICD as a calibration source. This choice has the drawback that the ICD does not provide a uniform illumination on the FOV of CAM, and considerable vignetting is seen at the edges of the detector (see § 6.1).

The ICD measurements were done throughout the mission, in all LW and SW filters, and at all PFOVs, except at 12$''$, where the ICD illumination would have been so high as to saturate the detector. A total of $\simeq$ 280 ICD FF measurements have been executed during calibration-dedicated rev.s, of which half with the SW detector. Additionally, at the end of every rev., a set of 4 FF ICD measurements were done routinely, in the SW1, SW3, LW2 and LW3 filters, with the purpose of constraining the long-term drifts. Full details on these measurements are given in Gallais (1998).

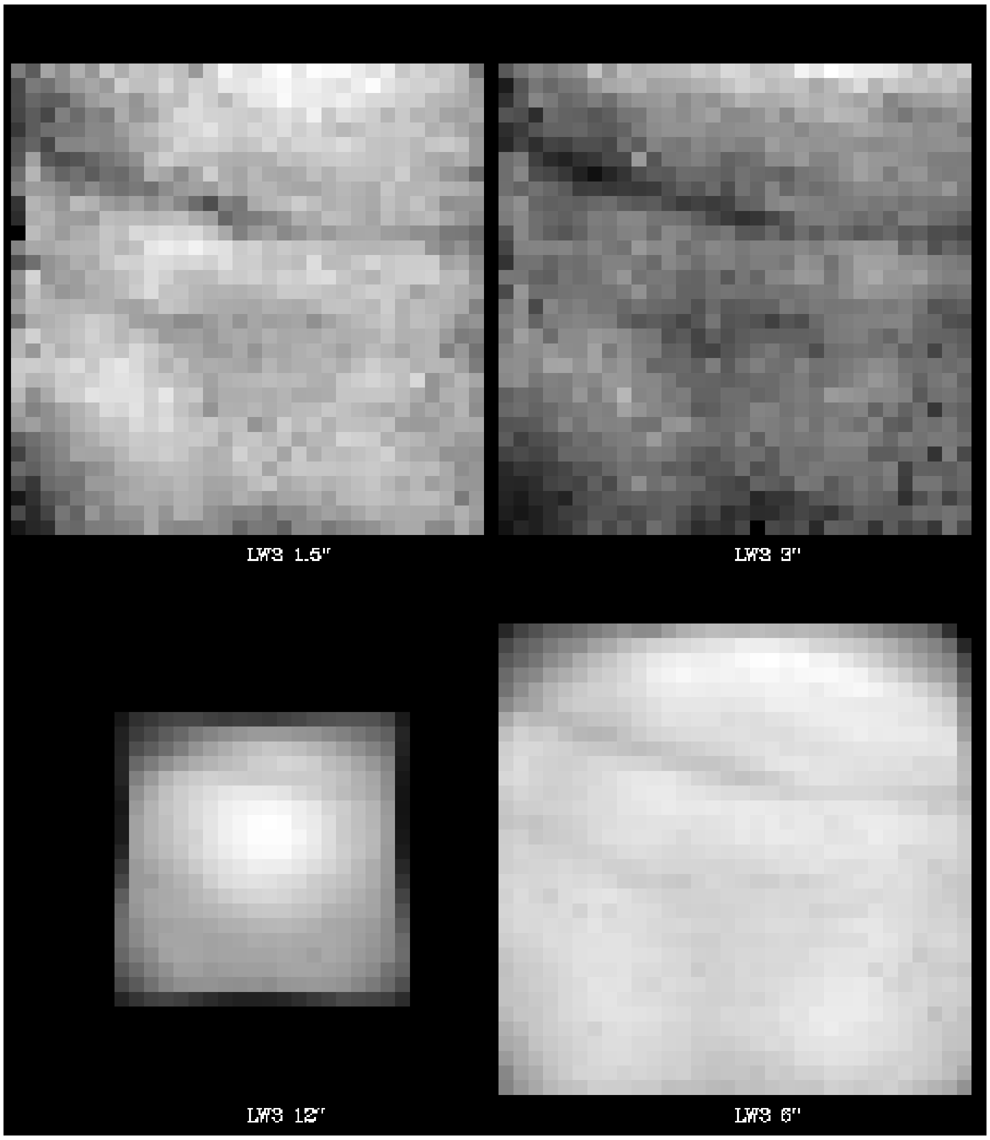

Figure 2: Four examples of ZB FFs in the LW3 filter. From top-left in clockwise order: 1.5″, 3″, 6″, 12″. Note that in the case of the 12″PFOV, only part of the array is illuminated.

2.2 Data reduction

The data-reduction for FF observations is done through the following steps:

- subtraction of the dark current;
- scaling of analog-to-digital units ("ADUs" hereafter) for the appropriate gain factor[1] and integration time used;
- deglitching;
- correction for transient behaviour;
- per-pixel median of all frames;
- normalisation of the final image by the mean flux in the central 11×11 pixels of the detector.

The dark-current subtraction has been done using the available CAL-G dark image, until the time-dependent dark-current model (Biviano et al. 1998a) became available, late in the mission. The noise coming from an inaccurate dark subtraction is reduced when the time-dependent dark-current model is used.

For deglitching, several CIA (Ott et al. 1996, Delaney 1997) methods have been used: *TCOR, TEMP,* and *MM.* Different methods have different advantages and disadvantages; however, in the case of FF data-redcution, the choice of the deglitching method does not seem to influence the final accuracy of the FF (see § 5.1).

The correction for the transient behaviour, on the other hand, *is* important. Several algorithms have been used in the data-reduction of FFs, until now, i.e. *S90, KSIG,* and *IAS* (for the LW detector only) under CIA. While the former two simply select those frames that are considered stabilized according to a given criterion, the *IAS* algorithm actually modifies the flux values according to a physical model of the detector (Abergel et al. 1996). As discussed in § 5.2, none of these algorithms can reduce the FF stabilization noise to zero. New algorithms are now being tested (e.g. Lari 1997).

After having taking the median of all frames, a normalisation is needed to reduce the FF image to dimensionless units. The normalisation factor is taken to be the average flux of the central 11×11 pixels, because the central part of the detector is not strongly affected by vignetting problems.

3 Long term trend

Gallais (1998) describes in detail the trend of the SW1, SW3, LW2 and LW3 FFs done with the ICD in the 1.5″ PFOV during deactivation. There is a scatter of ~ 3 % in the SW FFs and in the LW FFs. However, a large part of the scatter is due to a multi-modal distribution, that is clearly seen for SW, and is also present for LW. The origin of this multi-modal distribution is related to a wheel jitter (see Gallais 1998).

There are long-term drifts of $\simeq -0.8$ % per 100 revolutions in the four filters (the long-term trends are more irregular for the LW channel FFs). These trends are not very important for the calibration purposes, and prove that the median illumination of the detector and the median response to this illumination are quite stable throughout the whole ISO mission, at any wavelengths. So, both the ICD and the detector are stable, on average. This is also true when considering individual pixels separately.

[1] FF measurements are sometimes done with a gain factor ×1, and sometimes with a gain factor ×2. Here and in the rest of this document, all units are scaled by the gain factor *even if not explicitely indicated* – i.e. both "ADU" and "ADU/G" mean Analog-to-Digital Units scaled by the gain factor.

4 Characteristics of the calibration flat-fields

While very important for characterizing the long-term trend of the ICD and the detector responsivity, the deactivation FFs cannot be used for calibration. Infact, the deactivation FF images often show the remnants of previous observations occurred during the revolution, particularly when saturation occurred (see Gallais 1998). On the other hand, FF observations taken during the calibration-dedicated revolutions are done under very controlled conditions, and, as such, provide an excellent data-set. We here describe the level of accuracy that we have reached for the calibration FFs.

A minimum requirement for a useful measure of the FF, is to characterize each pixel responsivity better than the mean pixel-to-pixel variation. This variation can be characterized by the RMS of all pixel intensities relative to the median. In practice, this RMS value is a measure of the *flatness* of the image. This value has to be compared with an estimate of the accuracy level reached with calibration observations.

This accuracy can be characterized using the image-to-image per-pixel RMS flux[2] variation from several FF images obtained in different observations ("external" noise estimate), or using the frame-to-frame per-pixel RMS flux variation from a single observation ("internal" noise estimate). The median of all pixel RMS can then be taken to represent the global accuracy of the FF measurement.

There is a slight difference between the internal and the external noise estimates. The internal noise estimates are likely to underestimate the accuracy of the FF measurement, because they are based on *individual frames,* while the external estimates are based on the final FFs constructed from *a set of frames.*

This is indeed true in most cases, except for the regions of the array where illumination is lost because of the lens-wheel jitter. The lens-wheel position jitter sometimes displaces the CAM $6''$ per pixel beam off the large Fabry-mirror ("FM" hereafter), leading to a loss of signal on column 0, or sometimes column 31, of the array, as well as displacing the small FM inside the $3''$ per pixel beam. This leads to a loss of signal and a displacement of the FF, on the edges of the array, and since the jitter is random, different observations (at $6''$ with the large FM and at $3''$ with the small FM) have largely different illuminations at the edges (see Fig.3).

4.1 The SW channel

Let us now first consider the SW detector. As mentioned in § 2.1, the only estimates of the SW FFs come from the ICD measurements, since the zodiacal background flux at short wavelengths is not high enough. The RMS of the ICD SW FF image is typically 0.03–0.05 (in units of the median flux over the array), depending on the filter used. We measured the external per-pixel RMS using 83 ICD FF measurements. The median per-pixel RMS varies from 0.002 (in units of the median flux over the array) to 0.013, for the different SW filters, which means that the ICD FF accuracy is sufficient to characterize each pixel responsivity better than pixel-to-pixel variations. On the other hand, there may be a systematic error which is not accounted for by this analysis, since the ICD illumination of the detector is not uniform. In order to check this point, specific observations have been done, by observing a calibration star in different parts of the SW array, and by mapping a bright extended source. The data-analysis is ongoing.

[2]Note that since the measured flux varies according to the selected target region of the zodiacal background, one must use normalized units, i.e. all values are given in units of the median flux over the whole array.

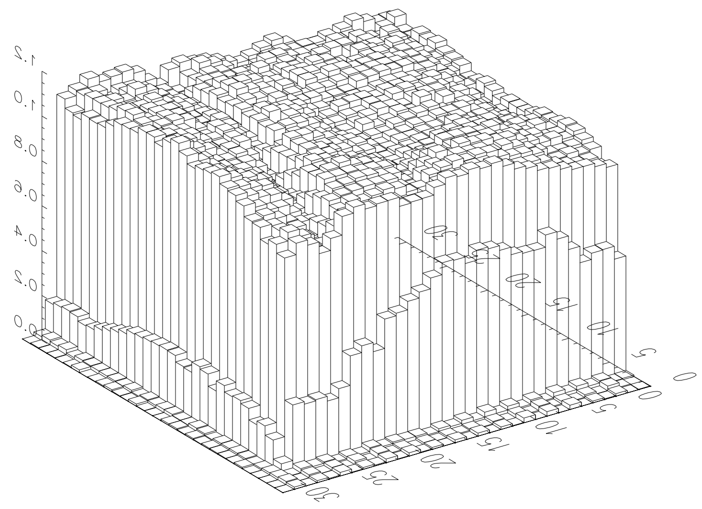

Figure 3: A rather extreme example of the effect of the lens-wheel jitter is given by this observation of the zodiacal background at 3.0″with the LW10 filter and the *small* Fabry mirror. The lens-wheel jitter displaces the CAM fov off the array by more than three pixels in one direction and more than two pixel in the orthogonal direction (so that the flux on cols. 0–2 and rows 30–31 is zero).

4.2 The LW channel

For what concerns the LW detector, the situation of the ICD FF measurements is similar to that described for the SW detector. However, we will see in § 6.1 and § 6.2 that the ICD-derived LW FFs are different from the ZB FFs, because of the non-uniform illumination from the ICD that causes significant vignetting. In order to obtain good measures of the FF, it is important to observe extended and uniform sources; since the ICD does not provide a uniform illumination over the whole array, one has to try to measure the FF by observing the zodiacal background.

The accuracy of the ZB LW FF observations have been estimated by comparing the internal RMS pixel-to-pixel flux variation in FF images, to the image-to-image per-pixel RMS flux variation, using 58 LW ZB FF observations.

It is convenient to characterize the internal RMS pixel-to-pixel variation (i.e. the flatness of the FF image) on the observations where the signal is highest, i.e. those made in the LW10 filter. We find the following values: 7 % for the 1.5″PFOV, 6 % for the 3.0″PFOV, 10 % for the 6.0″PFOV, and 29 % for the 12″PFOV, with respect to the median signal levels. The large RMS values found for the 6.0″ and 12″PFOVs FFs come from vignetting effects near the boundaries of the CAM FOV (edge effects, see § 4). These FFs are shown in Fig. 4, 5, 6, 7, respectively for the 1.5″, 3.0″, 6.0″, and 12″PFOV.

It is clear that in order to have a good estimate of the LW FF, each pixel responsivity must be characterized better than the pixel-to-pixel variations, i.e. the external per-pixel RMS from repeated observations, should be *at least* lower than $\simeq$ 6 %.

In Fig.8 we show the maps of the external per-pixel RMS for the LW10 ZB FFs at 1.5″, 3.0″and 6.0″PFOV. They were obtained after normalizing each FF image by its median flux value, in order to show only pattern – and not mean value – variations among different observations. Two plots are shown for the 3″PFOV, one to show the effect of the lens-wheel

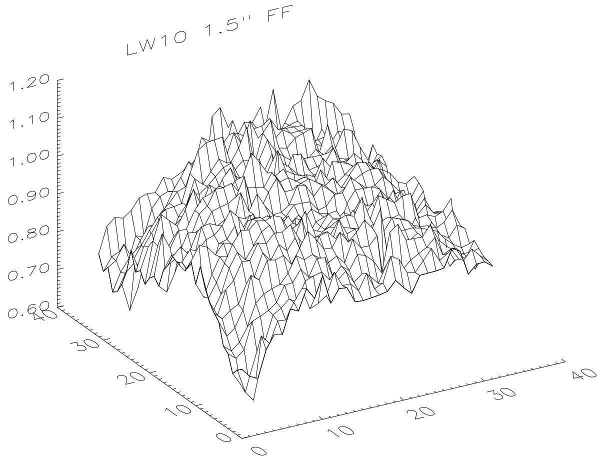

Figure 4: The 1.5″PFOV LW10 FF.

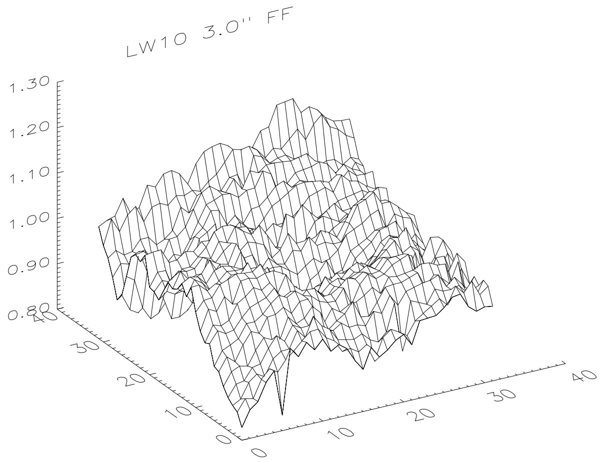

Figure 5: The 3.0″PFOV LW10 FF.

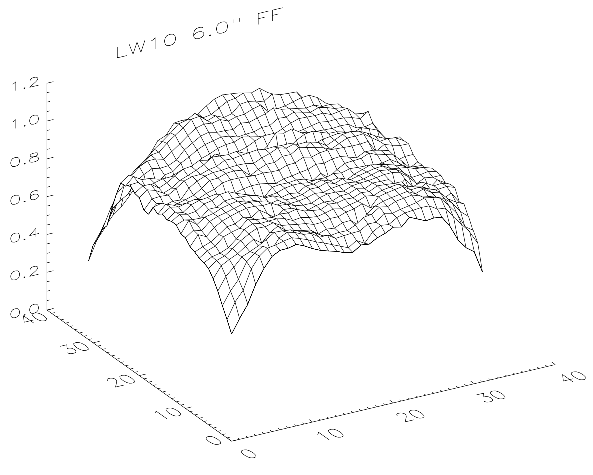

Figure 6: The 6.0″PFOV LW10 FF.

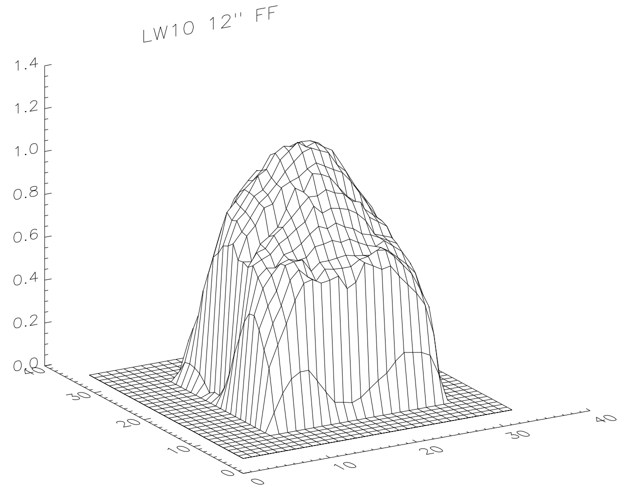

Figure 7: The 12.0″PFOV LW10 FF. Note that the external part of the array is not illuminated in this case.

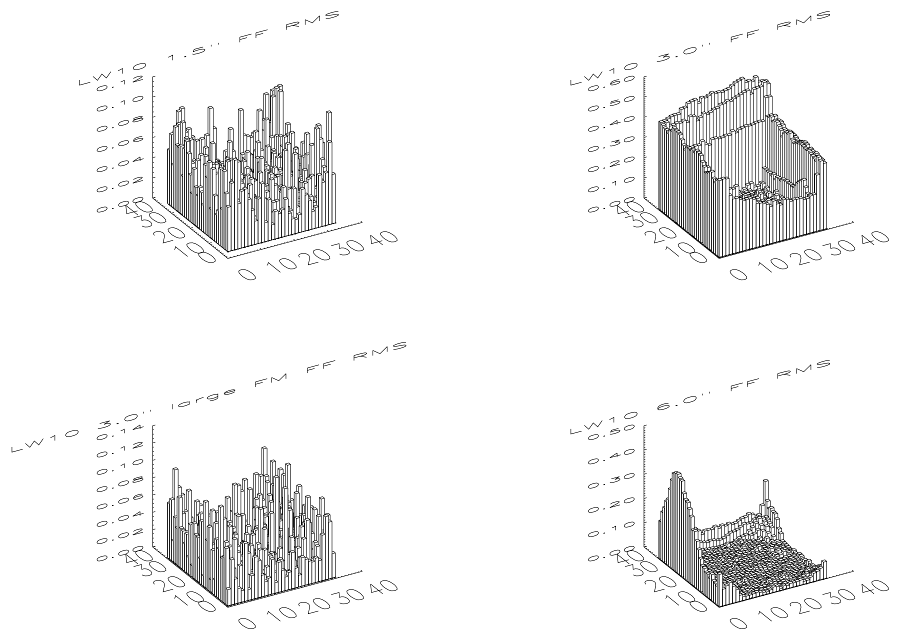

Figure 8: Per-pixel external RMS maps of FFs in the LW10 filter. Units on the z-axis are in fraction of the median FF flux. Top-left panel: 1.5″PFOV, top-right panel: 3.0″PFOV, bottom-left panel: 3.0″PFOV, large Fabry Mirror measurements only, bottom-right panel: 6.0″PFOV.

jitter on the edges of the detector, the other to emphasize the noise that is left once this jitter-induced noise has been taken away (either by considering only the central part of the array, or by considering – in the 3″PFOV case – only observations done with the large FM). If the effects of lens wheel jitter are not considered, the individual per-pixel fluctuations are ≤ 12 %.

Table 1 gives the current estimates of the per-pixel RMS noise for FFs of several configurations (note that not all configurations are yet covered by this analysis). We list the filter, the PFOV, the average flux (in ADU/s) of the image[3], and the resulting noise in units of the median flux. When we suspect that the jitter problem could have boosted the estimation of the external noise, the internal noise was listed instead. We also list the expected noise in terms of only the Read-Out noise and Poisson-noise contributions, and the noise arising from the dark subtraction, always with respect to the median flux detected. The dark noise contribution was estimated to be $\simeq 0.5$ ADU, i.e. twice the noise level that can be reached if a proper time-dependent dark current subtraction is done (Biviano et al. 1998a, Biviano 1998), because at the time these FF images were reduced, the time-dependent dark-current model was not yet available, so that the error associated to dark-subtraction is higher.

From the table, it is readily apparent that the per-pixel flux must be larger than ~ 2 ADU/s to provide an accuracy better than ~ 6 %, which is the minimum level we set for a ZB FF measurement that can be made use of. So, it seems virtually impossible to reach adequate signal/noise for ZB FFs in the LW1 and LW4 filters, essentially because the background is not bright enough, while in the LW3, LW8 and LW10 filters (all PFOVs) and in the 3″ and 6″PFOV LW2 configurations, the FF noise is below the RMS variation of

[3]When several FF images were available for a given configuration, we list here the maximum among the mean fluxes of all the images.

Table 1: Flat-field noise

Filter	PFOV$''$	<Flux> (ADU/s)	Noise	Read-out + Poisson-noise	Dark-noise
LW1	6.0	0.4	0.220	0.050	0.110
LW2	1.5	0.8	0.064	0.002	0.056
LW2	3.0	2.1	0.027	0.001	0.021
LW2	6.0	9.3	0.019	0.001	0.005
LW3	1.5	4.5	0.048	0.004	0.010
LW3	3.0	16.1	0.027	0.002	0.003
LW3	6.0	57.9	0.008	0.001	0.001
LW4	1.5	0.1	5.135	0.294	0.643
LW4	3.0	0.4	0.294	0.047	0.118
LW4	6.0	1.8	0.221	0.010	0.025
LW7	1.5	1.4	0.069	0.010	0.033
LW8	1.5	1.2	0.063	0.011	0.034
LW8	3.0	5.1	0.077	0.004	0.009
LW8	6.0	16.0	0.016	0.001	0.003
LW10	1.5	8.7	0.018	0.001	0.005
LW10	3.0	39.5	0.013	0.001	0.001
LW10	6.0	102.2	0.005	< 0.001	< 0.001

Table 2: OLP V.7 ZB FF CAL-G contents

PFOV$''$	Filters
1.5	LW3, LW10
3.0	LW2, LW3, LW6, LW7, LW8, LW9, LW10
6.0	LW2, LW3, LW4, LW6, LW7, LW8, LW9, LW10
12.0	LW3, LW6, LW8, LW9, LW10

pixel-to-pixel responsivity. Moreover, based on the flux received on a 1.5$''$ pixel, also the LW7 3$''$ and 6$''$ sky FFs may be good enough (but this remains to be checked on the data). The LW5 and LW6 filters are narrow and centered at relatively short wavelengths, so that the incident flux of the zodiacal background on the detector may not be high enough to provide an accurate FF characterization. The situation is probably more favorable for what concerns the LW9 filter, centered at 15 μm.

The results of this analysis are reflected in the contents of the LW FF CAL-G. Indeed, the signal-to-noise of calibration ZB FF images has driven the decision of whether to include or not these images into the calibration files that are provided to the observers. The contents of the FF CAL-G's in version 7 of the Off-Line-Processing are listed in Table 2. Note that the lack of 12$''$ZB FFs for some filters is not due to low signal-to-noise of the observations, but to the fact that not all the 12$''$ ZB FF observations have been reduced yet.

It is interesting to see how the noise level compares with that expected only on the basis of the Read-out, Poisson and dark-subtraction contributions. It is clear that the dark-noise dominates the FF noise at low signal levels (LW1, LW2 at 1.5$''$and 3$''$PFOVs, LW4, LW7 and LW8 at 1.5$''$PFOV). As discussed in Biviano et al. (1998a), the dark noise can now be reduced by 50 % by taking into account the long- and short-term drifts, so there is room for an improvement in some of the dark-noise-dominated FFs. For higher fluxes, the FF noise is no longer dominated by the dark-noise, but has an additional component. As it is well known (see e.g. Biviano 1998) the main sources of error for the CAM observations come from the glitch impacts and the transient response of the detector. So it is likely that either glitches or transients contribute to the error-budget of the FFs. See § 5.1 and § 5.2 for a detailed discussion of these effects in which we conclude that the additional main component of FF noise is not due to the glitch impacts, but rather to responsive transients.

As we will see below, stabilization may still be improved upon for the flat-fielding, i.e. calibration FFs are not *fully* stabilized. When stabilization is not achieved, a FF can be derived anyway, by taking into account only the last frames of the measurements. However, a compromise must be found between the need for having the most stabilized frames and the need for having enough frames. This is to say that a large amount of the observing time is spent for reaching stabilization.

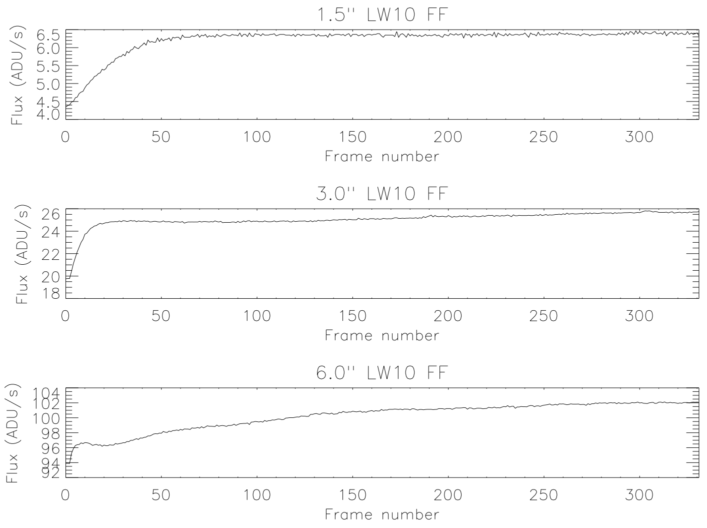

Figure 9: The median flux per frame of the zodiacal background FF measured in LW10 with T_{int} =5 s, during rev. 217, for three PFOVs: 1.5″(top panel), 3.0″(middle panel), 6.0″(bottom panel).

5 Error analysis

5.1 Effects of glitches

Several deglitching methods have been tried to ensure that undetected glitches are not affecting the FF estimation. We found that the RMS derived for different observations of the same configuration FF does not change if different deglitching methods are used.

Even if glitches are correctly removed, there is the additional transient effect of the glitch impacts which has to be accounted for. Glitches affecting the nominal sensitivity of the detector for several frames are called "dippers" (see Claret & Dzitko 1998). Pixels hit by dippers may not provide a correct estimate of the true FF value. However, dippers are relatively rare; since the calibration FF observations have typically several hundreds frames, and the FF is built by taking a median of all measurements, these glitch impacts should not be a major problem. We checked this, by considering the FF observed in the LW10 filter at 6″PFOV in rev.217.

We identified 19 pixels hit by (at least) one glitch that produced a sensitivity drop $\geq$ 10 ADU/s/frame, and 112 pixels hit by (at least) one glitch that produced a sensitivity drop $\geq$ 5 ADU/s/frame. After flat-fielding the FF image by a reference FF in the same configuration (obtained in rev.22), we computed the median RMS over all frames of all pixels, and the median RMS of all pixels except those (19 or 112) affected by a strong glitch impact. As expected, the RMS does not change when the pixels hit by dippers are removed.

We conclude that the glitches have no strong effect on the FF accuracy.

5.2 Effects of stabilization

In order to see if the FF images obtained within our current flat-fielding strategy are stabilized, we have looked at the time history through all the frames of their median flux (the median is taken over the whole array). In Fig.9 we plot the median flux as a function of the frame, for some LW10 ZB FFs, at 1.5″, 3.0″ and 6.0″PFOVs. Similar trends are found for other filter FFs. The 1.5″PFOV FF seems to have reached stabilization, while the others have not. However, this is not true as the following analysis shows.

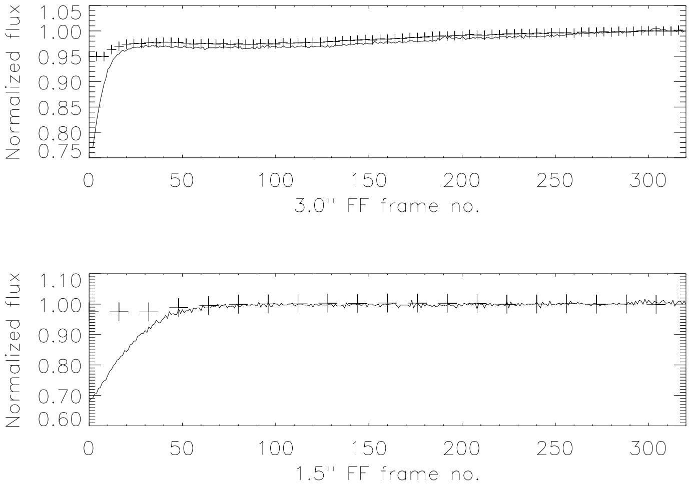

Figure 10: The median flux per frame of the zodiacal background FF measured in LW10 during the rev. no.217, at 6.0″(crosses) compared to the FF measured at the same sky position in different PFOVs: 3.0″(top panel) and 1.5″(bottom panel). To make a meaningful comparison, the time history of the 320 frames of the 3.0″FF has been compared to the first 80 frames of the 6.0″FF, and the time history of the 320 frames of the 1.5″FF has been compared to the first 20 frames of the 6.0″FF, because the long-trend stabilizing behaviour depends on the total per-pixel deposited flux. Units are normalized to the last considered frame (no.320 for the 3.0″and 1.5″PFOV FFs, and no.80 and no.20, for the 6.0″PFOV FF in the top and, respectively, bottom panel).

In order to compare the different PFOV FF time-histories, one must take into account the fact that the flux falling onto a pixel on a homogenous background is 4 times higher when using a 6.0″PFOV than a 3.0″PFOV, and 16 times when compared to a 1.5″PFOV. So, a 1600 s 1.5″ FF observation should correspond, in terms of deposited flux on the detector, to a 100 s observation with the 6.0″PFOV. As a consequence, a meaningful comparison for understanding the stabilization histories of our observations, is to compare the first 20 frames of the 1600 s 6.0″PFOV observation with the whole time-history (320 frames) of the 1.5″PFOV observation, and, similarly, the first 80 frames of the 6″PFOV observation with the 320 frames of the 3″PFOV observation. These comparisons are shown in Fig. 10. The fluxes have been normalized to the last frame considered (no.320 for the 3.0″and 1.5″PFOVs and no.80 or no.20 for the 6.0″PFOV, when this was compared to the 3.0″and, respectively, the 1.5″PFOV FF time-history). The similarity of the behaviours is striking, indicating that what seemed to be a stabilized 1.5″PFOV FF is not stabilized yet.

While most of ZB FF calibration observations lasted $\sim$ 1600 s, two were done with a much longer total integration time, $\sim$ 10000 s. We consider one of them, done in rev.22 at 6.0″PFOV in the LW10 filter, in order to analyze the stabilizing trend after the first 1600 s. The median flux vs. frames of this very long observation is shown in Fig.11. It can be seen that, after an initial upward stabilization and after a final level seems to be reached, the signal turns down again after the frame 2000. Even this very long lasting observation does not seem to have produced a *fully* stabilized FF! In reality, the decrease of the median FF flux after the frame 2000 is *not* due to incomplete stabilization, but to the change of the LW detector sensitivity through the orbit (see Biviano 1998, and Blommaert 1998), so the FF median flux is indeed stabilized after $\sim$ 4000 s observing time.

It is important to get an estimate of the noise that incomplete stabilization induces in FFs. Until now we have looked at the stabilization trend of the median value over the array. Of course, the FF pattern would be unaffected by incomplete stabilization if *all* pixels stabilize

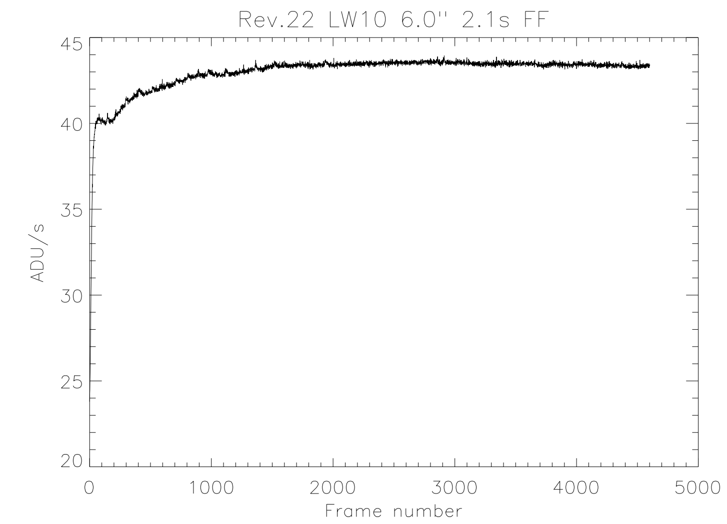

Figure 11: The median flux of the ZB FF measured with T_{int} =2 s, during the rev. no.22, vs. frame, at 6.0″PFOV. The total observation lasted $\sim 10^4$ s.

exactly in the same way. But stabilization is unlikely to proceed like that, because different pixels have different sensitivities, and they may respond differently to an identical incident flux. In order to understand how much of the FF noise is due to incomplete stabilization, we have considered the long-exposure ZB FF done in rev.22.

We want to estimate how much of the noise we see in our typical FFs can be due to incomplete stabilization. We can do that by slicing the rev.22 FF into 10 FFs, the 1st constructed from the frames from 0 to 460, the 2nd from frame 461 to 920 and so on. We then used the 10th FF (the one built upon the most-stabilized frames) as a *reference* FF and divide the previous 9 FFs by it. The analysis of the residual noise in the resulting "flat-fielded flat-fields" should give us an indication of how much does incomplete stabilization increase the noise in a FF.

The median RMS over the array of these FFs decreases from 2.6 % to 1.6 % and 0.8 % in going from the 1^{st} to the 2^{nd} and finally to the 9^{th}. This is also shown graphically in Fig.12. The calibration ZB FFs are typically comparable to the 2nd bin FF, in terms of observing-time, so that by comparing the RMS noise in the 2^{nd} bin FF to the noise in the 9^{th} bin FF, we can conclude that as much as 0.8 % of our typical FFs is due to incomplete stabilization. As this is an "internal" noise, it may again be a slight overestimate. However, this value is strictly valid only for the configuration considered (LW10 6.0″) and for other configurations the stabilization noise may be larger. It is interesting to note that this stabilization noise can account for all of the LW10 6.0″residual noise after accounting for the Read-out, Poisson and Dark-subtraction noise (see Table 1).

In principle, one would like to be able to correct for this incomplete stabilization. We have tried such a correction using the model of Abergel et al. (1996) on six LW10 6″FF observations, but there was no improvement at all (the external median RMS among the six FF images remained the same). This failure is not unexpected, since the model is suited to correct for fast transients (with a time constant of 0.6/flux seconds), not for the long-lasting ones. Possibly, new models (Lari 1997) could improve the current situation.

In the end, this analysis stresses that, while it is possible *in principle* to obtain better FFs by observing longer, this is in practice unfeasible; our typical ZB FF observations already last 1600 s, and given the many possible CAM configuration FFs, they could not have been lasting much longer except at the expense of other important calibration measurements (e.g.

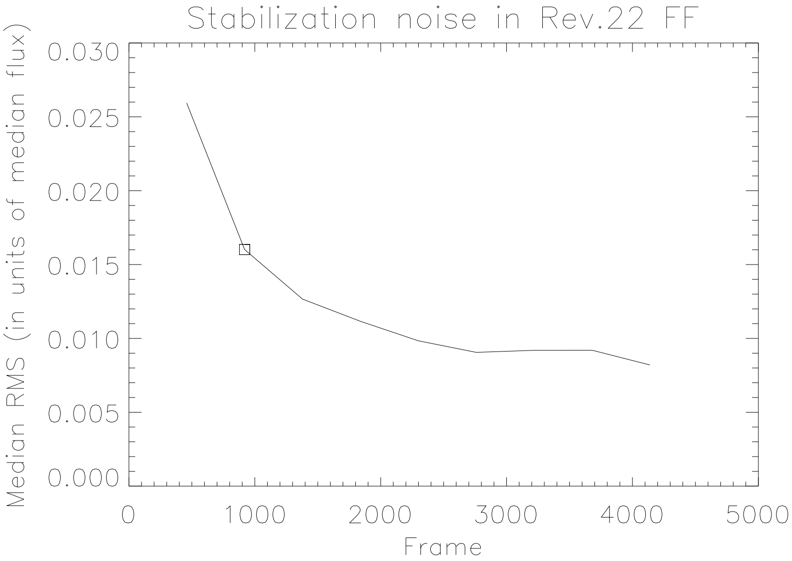

Figure 12: The internal RMS noise of a FF as obtained from different subset of the rev.22 ZB FF frames. The y-axis is the RMS noise in units of the median flux over the array, after the FF has been flat-fielded by a reference (most stabilized) FF. The x-axis represents the frames over which the FFs have been computed (i.e. the first point is obtained from the flat computed on frames 0–460, the second on frames 461-920, and so on). The square indicates the location on the stabilization noise curve of a typical calibration ZB FF that lasts $\sim$ 1600 s.

photometry). However the achieved accuracies in the long-wavelength filters (where the sky signal is high enough) are already quite similar to what was targeted before launch.

6 Strategies for flat-fielding calibration

In § 5.2 we have shown that incomplete stabilization accounts for that part of the FF RMS error that is not accounted for by the dark, Poisson and read-out noise. However, in many configurations the zodiacal background flux per pixel is simply too low to allow the FF characterization. Let us stress again that rasters and beam-switch observations generally provide their own FFs and so the problem of accurate flat-fielding arises only for some observers using staring mode who happen to be unlucky in perhaps encountering an unfavourable manifestation of the wheel jitter effect in CAM, causing their data to be poorly compatible with library FFs. We nevertheless need to consider what can be done to reach a better FF accuracy for the CAM configurations for which the per-pixel sky flux is too low. Here we present possible solutions to this problem, and discuss their relative advantages and disadvantages.

6.1 Exportable optical flat

As discussed in § 1, one can think of a given configuration FF as the product of a DF that depends on the filter (the detector responsivity depends on the wavelength) and of an OF that depends on the optical configuration, but (in principle) not on the filter.

As a consequence, if, in a given filter, the zodiacal background flux is high enough on a $6.0''$ pixel, but not on a $1.5''$ pixel, it is possible to use the measured ZB $6.0''$ FF and divide it by an independent measure of the $6.0''$ OF to obtain the DF, i.e. the FF at $1.5''$. The trick here is that if the OF is really the same for all filters, one can use an OF derived using other sky FF observations with long-wavelength filters (LW3 or LW10), or an OF derived for the specific filter using ICD observations.

This has been tested by comparing the ZB LW3 OF with the ZB LW10 OF and with the median ICD OF of all filters. Using the error-map of the ratio between the ZB LW3 OF and the ZB LW10 OF (derived from the individual RMS maps of the LW3 and LW10 OFs, via the propagation-of-error analysis) we can see whether or not this ratio is significantly different from one, for individual pixels. We found that the ratio between the ZB LW3 OF and the ZB LW10 OF is significantly different from one (at 2 σs) for 6 % and 17 % of the pixels at 3.0″and 6.0″PFOV, respectively. This is higher than expected from a gaussian distribution. The median value of the ratio of the two OFs for all pixels is 1.00 for the 3″PFOV and 1.01 for the 6″PFOV, with maximum values of ~ 1.3 in both PFOVs.

We found a similar result for what concerns the ratio between the ZB LW10 OF and the ICD OF, although in this case the difference is higher for the 6.0″PFOV than for 3.0″PFOV. The median and maximum values of the ratio of the LW10 OF and the median ICD OF, are 1.02 and 1.27 at 3.0″, and 1.11 and 12.58 (!) at 6.0″. The huge deviation from unity found for the ratio between LW10 and the ICD OFs is due to edge-effects introduced by the non-uniform illumination of the detector by the ICD. This is illustrated in Fig. 13.

So it looks like the OF from one filter is not exportable to another filter without the introduction of additional noise, and the same is true for what concerns the exportability of ICD OFs to ZB OFs. The difference between the ZB OF and the ICD OF must come from the non-uniform illumination of the ICD, but the slight difference between different filter OFs is unexpected. The reason of this difference may lie in residual straylight contamination that is difficult to quantify (as suggested by Perault & Metcalfe 1995; see also Okumura 1998 and Biviano et al. 1998b).

Summarizing, if a 6.0″or 3.0″FF ZB measurement is available for a given filter, yet the 1.5″FF is not (because the per-pixel flux is too low), it is possible to use the OF as measured on the sky in another filter where the zodiacal flux is higher (either because the filter is centered at a higher wavelength or because the filter bandpass is wider), to derive the DF from the measured 3.0″or 6.0″ ZB FF. Using the OF as measured with the ICD is not a better choice, since it introduces strong edge effects. Using the OF from another filter may however introduce a slight additional noise in the final FF (~ 1 % on average).

6.2 Exportable detector flat

When the zodiacal background flux is low even on a 6.0″ pixel, there is no other choice than using the ICD or the ZB FF from another filter.

We have checked the similarity of the ICD and ZB DFs of the LW10 and the LW3 filters. The comparison was done for these filters because their ZB FFs are the best determined among all CAM filters. In Fig. 14 we plot the deviation from unity of the ratios of the ZB DF to the ICD DF in both the LW3 and the LW10 filters.

In order to check the significance of the differences between the ZB and ICD DFs we computed the RMS map of the image of the ratio of the two, from the RMS of both images (via the propagation-of-error analysis). The ratio between the ICD and the sky LW10 (LW3) FF is significantly different from unity at more than 2 σs for 22 % (47 %) of the pixels. This means that the ICD and the sky observations give FFs that are significantly different on a consistent fraction of the array. The median and maximum values of the ratio of these DFs is 1.03 (1.05) and 1.18 (1.32) for the LW10 (LW3) filter. So, on average, using the ICD FF instead of the ZB FF introduces an additional error of ~ 4 %.

For what regards the exportability of the sky DF from one filter to another, we have compared the LW2 and LW3 DF to the (more accurate) LW10 DF. The ratio between the LW2 and the LW10 DFs is significantly (more than 2 σs) different from unity in 18 % of the pixels, while the ratio between the LW3 and LW10 DFs is significantly different from unity

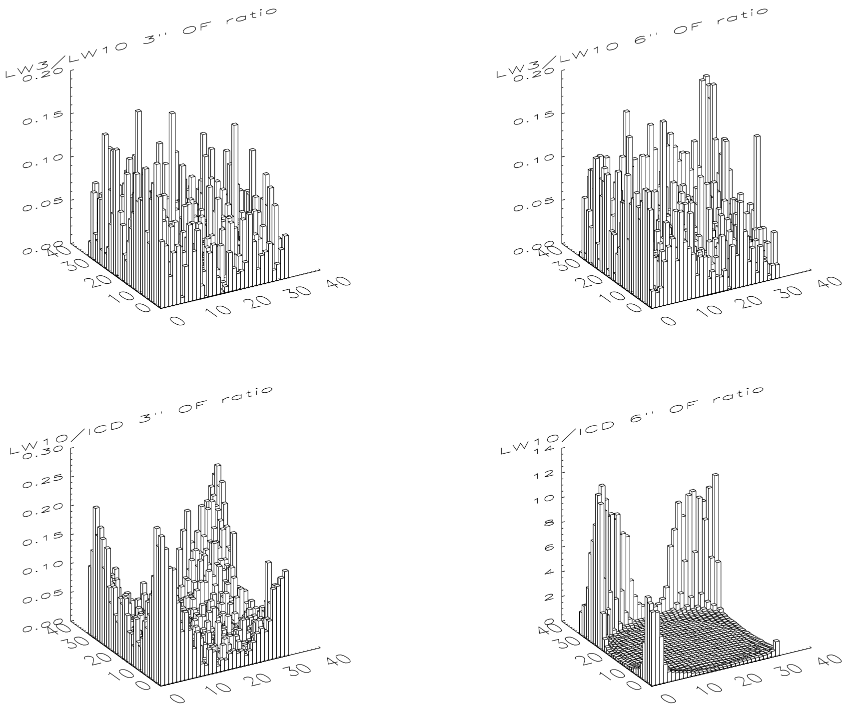

Figure 13: Optical Flat ratios. Top panels: deviation from unity of the ratio between the LW3 and the LW10 ZB OFs at 3.0″(left) and at 6.0″(right). Bottom panels: deviation from unity of the ratio between the LW10 ZB OF and the median ICD OF of all filters at 3.0″(left) and at 6.0″(right).

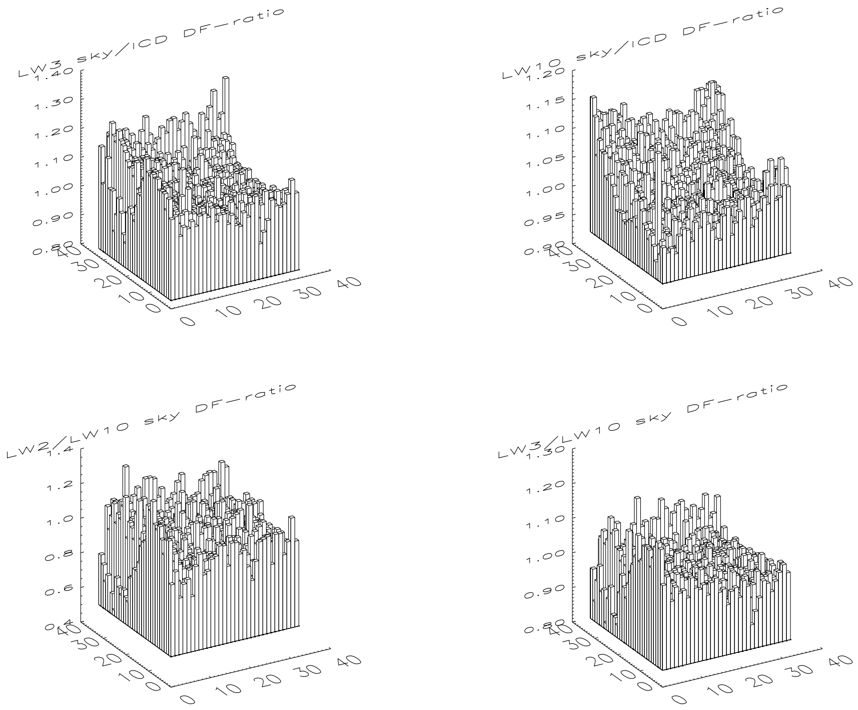

Figure 14: Top-panel: the deviation from unity of the ratio between the ZB DFs and the ICD DFs in the LW3 filter (left) and in the LW10 filter (right). Bottom panel: the deviation from unity of the ratio between the LW2 and LW10 ZB DFs (left) and between the LW3 and LW10 ZB DFs (right).

only in 7 % of the pixels. The fact that the LW3 and LW10 DFs are more similar than the LW2 and LW10 DFs is not unexpected, since the central wavelenghts of the LW3 and LW10 filters are more similar than those of the LW2 and LW10 filters, and we expect the pixel responsivities to have a dependence on the wavelength of the incident radiation.

The ZB DF of one filter can be exported to another filter only at the price of an additional error. This is estimated from the median (maximum) deviation from unity of the ratio of the two filter DFs, which is 6 % (42 %) for the LW2/LW10 ratio, and 1 % (29 %) for the LW3/LW10 ratio.

So, on average, the DF can be exported from a filter to another by the expense of an additional error of ~ 6 % or lower (if the filters have similar wavelengths).

7 Conclusions

We have shown that the accuracy with which we can derive FFs from ZB observations is either limited by incomplete stabilization, or by the low ZB flux level (in which case the dominant source of error is the dark subtraction).

In the former case, we have shown that reaching the Poisson-noise-dominated regime needs very long observations (~ 2 hours). The limited time available for calibration observations and the large number of calibration issues have not allowed us to spend such a long time on FF observations. However, the average time spent for FF calibration observations is appropriate to beat much of the stabilization error.

In the latter case, we have considered alternative approaches to the direct measurement of the FF on the sky, such as using the ICD FFs, or exporting the OF and/or the DF from other filters where the illumination is higher. While these approaches do introduce additional noise, this is not large, so that these strategies for flat-fielding calibration look appropriate.

For what concerns the SW channel, in no filter do we have a zodiacal background measurement of the FF, because the zodiacal background is not bright enough. Flat-fielding in the SW channel can only be based on the ICD measurements. Since the ICD illumination of the detector is not uniform, it is nevertheless important to give even a sparse sampling of the SW FF by other means. A calibration star has been mapped over the SW array with this purpose, and the analysis of this observation is ongoing.

It is important to stress again that most raster and beam-switch CAM scientific observations can provide independent FF estimations. The idea behind these observing modes is indeed to beat the pixel-to-pixel variation by observing the same sky region with different pixels. Observers using these observing modes do not need to be particularly concerned about the quality of the calibration FFs. The calibration FFs are however necessary for staring observations (or when the source is very extended with respect to the raster size, or the observed field is very crowded).

Imperfect flat-fielding induces two kind of errors: the photometric error arising from the uncertainty in the responsivities of the pixels that see the source, and the photometric error arising from the background subtraction. As the source will be usually located at the centre of the array, the former error will always be relatively low, of order few percents, even when no sky FF is available, since one can safely use the ICD FF. On the other hand, identifying faint sources over a high-brightness background requires a very accurate FF.

As an example, the currently achieved median accuracy of 0.5 % in the LW10 $6''$FF means that with an average background flux of 50 ADU/s in this configuration, the 1-σ limit for the detection of a faint source per pixel is $\sim 60\mu$Jy (using the ADU/s to Jy conversion factors from Blommaert 1998). On the other hand, the poor accuracy of only 6 % that we have reached for the LW2 $1.5''$FF gives a 1-σ limit per pixel of $\sim 20\mu$Jy for a typical background flux of 0.8 ADU/s in this configuration. In other words, in the configurations where the background flux is high we need a higher FF accuracy, but if the flux is high a higher ZB

FF accuracy is easier to met.

We therefore consider that pre-launch expectations of $\sim$ 1–3 % in the FF accuracy (Perault & Metcalfe 1995) have been met, since when this accuracy is needed (long-wavelength filters) calibration FF accuracies are of this order of magnitude (and possibly better in some cases).

References

Abergel A., Désert F.-X., Aussel H. 1996, "IAS model for ISOCAM LW transient correction"

Aussel H. 1997, in preparation

Biviano A. 1998, "The ISOCAM calibration error budget"

Biviano A. et al. 1998a, "The ISOCAM dark current calibration report"

Biviano A. et al. 1998b, "The ISOCAM CVF calibration report"

Blommaert J. 1997, "ISOCAM photometry report"

Boulade O. 1996, "CAM report on pointing jitter"

Claret A. & Dzitko H. 1998, "ISOCAM glitch library"

Cohen M., Witteborn F., Walker R., Bregman J., Wooden D. 1995, AJ 110, 275

Delaney M. 1997, "ISOCAM interactive analysis user's manual", v.2.0

Gallais P. 1998, "Report on the trend analysis of the CAM daily calibration measurements"

Lari C. 1997, "IRA model for ISOCAM LW transient correction"

Okumura K. 1997, "ISOCAM PSF report"

Ott S. et al. 1996, "Design and implementation of CIA, the ISOCAM interactive analysis system", ASP conference series vol.125

Perault M., Metcalfe L. 1995, "Technical note about the error budget estimate in CAM observations"

Salama A. 1996a, "Report on the Rev.264 ISO pointing accuracy experiment"

Salama A. 1996b, "The Rev.368/369 ISO STR calibration adjustement verification experiment"

List of abbreviations and symbols

- ADU, ADU/G, ADU/g - Analog to Digital Unit, the unit of all CAM observations, scaled by the gain factor;
- CVF - Circular Variable Filter;
- DF - Detector Flat;
- FF - Flat Field;
- FM - Fabry Mirror;
- g, G - Gain;
- ICD - Internal Calibration Device;
- OF - Optical Flat;
- PFOV - Pixel Field-Of-View;
- PSF - Point Spread Function;
- rev. - revolution;
- s, sec - second, unit of time;
- T_{int} - the integration time of a single frame exposure;
- ZB - Zodiacal Background.